Available online at www.sciencedirect.com
SCIENCE DIRECT
ELSEVIER
Geomorphology 1432 (2003) xxx–xxx
GEOMORPHOLOGY
www.elsevier.com/locate/geomorph

Landscape disequilibrium on 1000–10,000 year scales Marsyandi River, Nepal, central Himalaya

Beth Pratt-Sitaula[a,*,1], Douglas W. Burbank[a,1], Arjun Heimsath[b], Tank Ojha[c]

[a] Department of Geosciences, Pennsylvania State University, University Park, PA 16802, USA
[b] Department of Earth Sciences, Dartmouth College, Hanover, NH 03755, USA
[c] Himalayan Experience, PO Box 5674, Kathmandu, Nepal

Received 1 October 2002; received in revised form 14 July 2003; accepted 16 July 2003

Abstract

In an actively deforming orogen, maintenance of a topographic steady state requires that hillslope erosion, river incision, and rock uplift rates are balanced over timescales of 10^5–10^7 years. Over shorter times, $<10^5$ years, hillslope erosion and bedrock river incision rates fluctuate with changes in climate. On 10^4-year timescales, the Marsyandi River in the central Nepal Himalaya has oscillated between bedrock incision and valley alluviation in response to changes in monsoon intensity and sediment flux. Stratigraphy and ^{14}C ages of fill terrace deposits reveal a major alluviation, coincident with a monsoonal maximum, ca. 50–35 ky BP. Cosmogenic ^{10}Be and ^{26}Al exposure ages define an alluviation and reincision event ca. 9–6 ky BP, also at a time of strong South Asian monsoons. The terrace deposits which line the Lesser Himalayan channel are largely composed of debris flows which originate in the Greater Himalayan rocks up to 40 km away. The terrace sequences contain many cubic kilometers of sediment, but probably represent only 2–8% of the sediments which flushed through the Marsyandi during the accumulation period. At $\sim 10^4$-year timescales, maximum bedrock incision rates are ~ 7 mm/year in the Greater Himalaya and ~ 1.5 mm/year in the Lesser Himalayan Mahabarat Range. We propose a model in which river channel erosion is temporally out-of-phase with hillslope erosion. Increased monsoonal precipitation causes an increase in hillslope-derived sediment that overwhelms the transport capacity of the river. The resulting aggradation protects the bedrock channel from erosion, allowing the river gradient to steepen as rock uplift continues. When the alluvium is later removed and the bedrock channel re-exposed, bedrock incision rates probably accelerate beyond the long-term mean as the river gradient adjusts downward toward a more "equilibrium" profile. Efforts to document dynamic equilibrium in active orogens require quantification of rates over time intervals significantly exceeding the scale of these millennial fluctuations in rate.

Keywords: Cosmogenic dating; Landscape evolution; Marsyandi River; Monsoons; Fill terrace; Bedrock incision

1. Introduction

Since Hack (1960) revived the idea of dynamic equilibrium in landscapes (Gilbert, 1877), geomorphologists have placed much emphasis on the implied equilibrium or balance in topography. Although

* Corresponding author. Tel.: +1-805-893-7242; fax: +1-805-893-2314.
E-mail address: pratt@crustal.ucsb.edu (B. Pratt-Sitaula).
[1] Present address: Department of Geological Sciences, University of California, Santa Barbara, CA 93117, USA.

0169-555X/$ - see front matter © 2003 Published by Elsevier B.V.
doi:10.1016/j.geomorph.2003.07.002

the dynamic nature of natural systems is well recognized, studies of orogenic evolution commonly ignore short-term unsteadiness. Assumptions that river incision rates define regional erosion rates (e.g. Tucker and Slingerland, 1996; Willett, 1999), that erosion is balanced by rock uplift (e.g. Synder et al., 2000; Kirby and Whipple, 2001), or that erosion rates can be considered constant (e.g. Small et al., 1997; Hancock et al., 1998) simplify many geomorphic problems and facilitate predictions about the evolution of landforms under various conditions.

Over extended times ($\geq 10^6$ year), many orogenic landscapes appear to achieve equilibrium shapes with rock uplift balancing erosion (e.g. Burbank et al., 1996; Pazzaglia and Knuepfer, 2001). However, many of the observable variables (such as river-borne sediment flux, hillslope angle, active processes, or channel width) are subject to the dynamic forcing of climate, episodic uplift, and other irregularly varying controls (e.g. Schumm, 1973; Tucker and Slingerland, 1996). The fluctuations around the hypothetical equilibrium are the commonly observable conditions. But what is the range of perturbation? To properly interpret such observations, the size, nature, and timescale of the dynamic swings about the equilibrium must be quantified.

In many rapidly eroding orogens, the range, timing, and interplay of channel sedimentation and incision are poorly known. The steep valley walls, narrow bedrock river channels, and absence of significant modern sediments storage serve to focus attention on the process of incision in active orogens (e.g. Burbank et al., 1996; Stock and Montgomery, 1999; Lavé and Avouac, 2000). However, even within many active orogens, flights of aggradational terraces show that this process is periodically reversed (e.g. Bull, 1991; Porter et al., 1992; Lavé and Avouac, 2001). Both incision and aggradation must, therefore, be evaluated when extrapolating long-term rates and processes.

This study investigates the range and timing of channel sedimentation and incision in central Nepal, a region with known long-term denudation rates. Due to a potent interplay between climate and tectonics, this is an excellent study area for understanding how much a natural system oscillates around its million-year average. Using detrital $^{40}Ar/^{39}Ar$ dating from the Marsyandi main trunk and tributaries as well as numerical analysis, Brewer (2001) determined that the Marsyandi catchment in the Greater Himalaya experienced an average vertical denudation rate of ~ 1.5–2 mm/year over the last 5–10 My. With hillsides generally hovering around the threshold angle for landslide failure, the bedrock river incision rate should control the rate of landscape lowering (Carson and Kirkby, 1972; Burbank et al., 1996). We infer that on the million-year timescale, the Greater Himalayan reach of the Marsyandi River should be incising at a pace similar to 1.5–2 mm/year. Using cosmogenic dating of polished fluvial surfaces, ^{14}C dating of deposits, and fill terrace stratigraphy, we test whether this long-term denudation rate is observable on shorter timescales.

2. Background

2.1. Study area

The Marsyandi River is a trans-Himalayan river ~ 120 km NW of Kathmandu in central Nepal. With headwaters on the southern edge of the Tibetan plateau, it cuts between the >8000-m-high peaks of Annapurna and Manaslu and flows into the monsoon-soaked Lesser Himalaya, draining an area of ~ 4800 km^2 (Fig. 1). The study area extends from the Upper Marsyandi, north of the Greater Himalaya, to the confluence with the Kali Gandaki in the lowlands to the south.

2.2. Regional geology

Along its route, the Marsyandi traverses the four main tectonic units of the central Himalaya (Fig. 2). Not surprisingly, major changes in topography, hillslope angle, and lithology are associated with contrasts between these large-scale tectonic units. Understanding the differences between these units allows for better assessment of the ongoing geomorphic processes.

North of the Greater Himalaya, the more readily eroded rocks of the Tibetan Sedimentary Sequence overlie medium- and high-grade gneisses of the Greater Himalayan Sequence along the Chame detachment (Hodges et al., 1996). The Main Central Thrust, a ductile shear zone just south of the main Himalayan relief, carries Greater Himalayan Sequence rocks over the lower-greenschist to lower-amphibolite

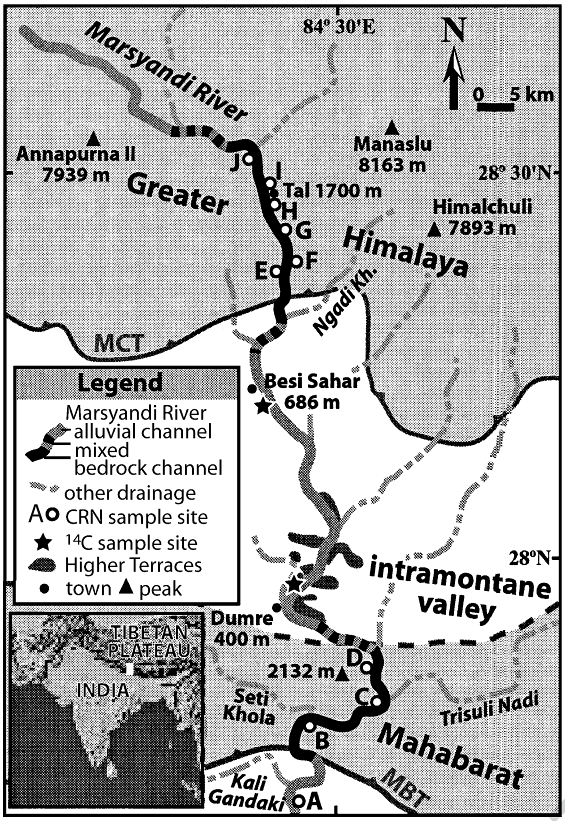

Fig. 1. Sample site locations, Higher Terraces, and major structures in the study area. MCT, Main Central thrust; MBT, Main Boundary thrust; CRN, cosmogenic radionuclide.

facies rocks of the Lesser Himalayan Sequence (e.g. Hodges, 2000). On the southern margin of the Lesser Himalaya, the Mahabarat Range overthrusts the Neogene molasse to the south along the south-vergent Main Boundary thrust. The current southern limit of deformation is characterized by the thin-skinned tectonics of the Main Frontal thrust, ~ 50 km south of the Main Boundary thrust (Nakata, 1989).

The Main Frontal thrust, Main Boundary thrust, and Main Central thrust are interpreted to merge at depth with the Main Himalayan thrust. The Main Himalayan thrust is commonly interpreted to have a 20–25° ramp beneath the Greater Himalaya and flatter ramps to the north and south (Ni and Barazangi, 1984; Molnar, 1987; Pandey et al., 1995) (Fig. 3B). Given the ~ 20 mm/year convergence between Peninsular Indian and southern Tibet (Bilham et al., 1997), Brewer (2001) showed that the observed cooling-age distribution in the Marsyandi catchments is best explained by partitioning the convergence into 5 mm/year of Asian overthrusting and 15 mm/year of Indian underthrusting. Five millimeters per year of thrusting over a 20–25° ramp should lead to 1.5–2 mm/year rock uplift.

2.3. Geomorphology

The modern Marsyandi River valley can be divided four main reaches—an alluvial portion north of the Greater Himalaya; a bedrock reach that cuts across the Greater Himalayan divide; an ~ 70-km-long stretch of alluvial channel in the intramontane valley south of the main topographic front; and another reach of

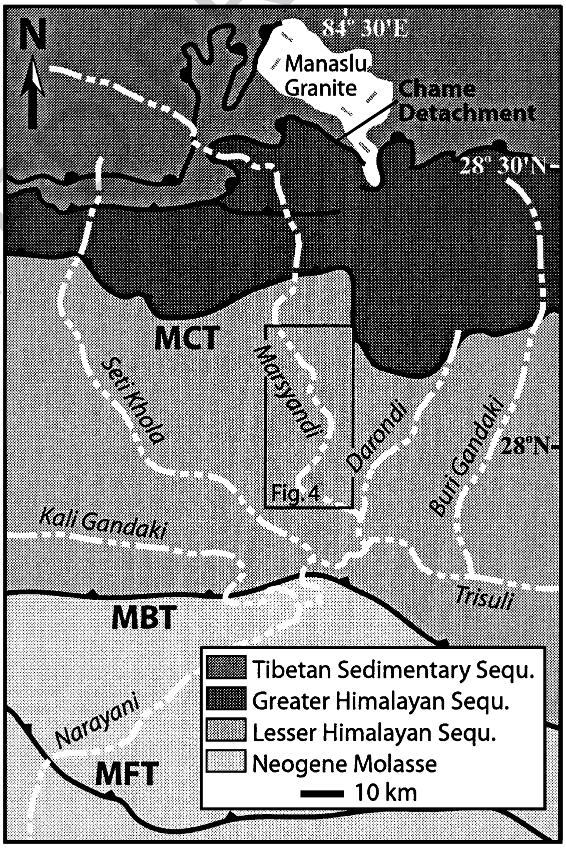

Fig. 2. Schematic geological map of the study region adapted from Hodges et al. (1996), Colchen et al. (1986), and Lavé and Avouac (2000). MCT, Main Central thrust; MBT, Main Boundary thrust; MFT, Main Frontal thrust. Fig. 4 maps major alluvial terraces.

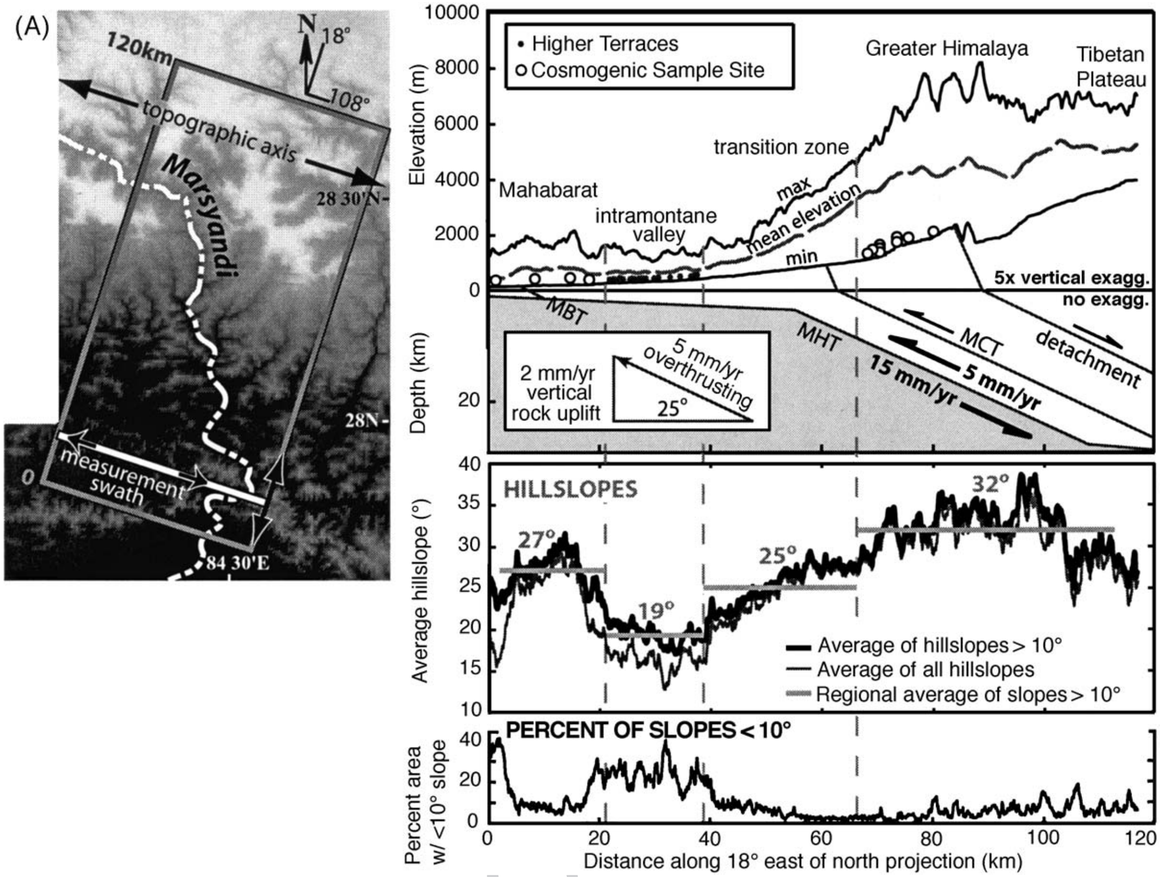

Fig. 3. Elevation and hillslope angle across the Marsyandi region. (A) The extent of the 3-arcsecond digital elevation model (DEM) over which elevations and slopes were averaged. Measurement swaths are oriented parallel to the 108° central Himalayan regional topographic axis. (B) Maximum, mean, and minimum elevations with a schematic cross-section of major structures and locations of Higher Terraces and cosmogenic radionuclide sample sites; 5 mm/year Asian over thrusting along a 20–25° ramp creates 1.5–2 mm of vertical uplift. Modified from Brewer (2001). (C) Average hillslope angles: all slopes and slopes >10°. (D) Percent of slopes < 10°. MCT, Main Central thrust; MBT, Main Boundary thrust; MHT, Main Himalayan thrust.

bedrock channel where the river flows through the 2000-m-high Mahabarat Range and joins the Trisuli, Seti, and Kali Gandaki Rivers. Analysis of 3-arc-second digital topography (~ 90-m cells) reveals similar subdivisions (Fig. 3). The intramontane alluvial reach corresponds to a region of low mean hillslope angles and low topographic relief, as well as a high frequency of hillslopes < 10°. Higher slope angles, greater relief, and a low frequency of slopes < 10° correspond to bedrock reaches in the Mahabarat and Greater Himalaya.

The bedrock reaches of the Marsyandi within the Greater Himalaya and the Mahabarat are characterized by narrow V-shaped valleys whose walls hover close to the critical angle (>30°) for landslide (Fig. 4C). In many places, the channel has a veneer of alluvial cover, but with one preserved up to 125 m above the modern river level. Stranded sedimentary deposits along the bedrock reaches are typically thin and restricted to tens to hundreds of meters in lateral extent. A few remnants are found as high as 120 m above the modern river.

The Marsyandi alluvial reaches occur in wider, less-sheer valleys containing extensive fluvial and debris deposits. North of the Main Himalaya, most of the deposits are diamictons up to several kilometers in down-valley extent and several hundred

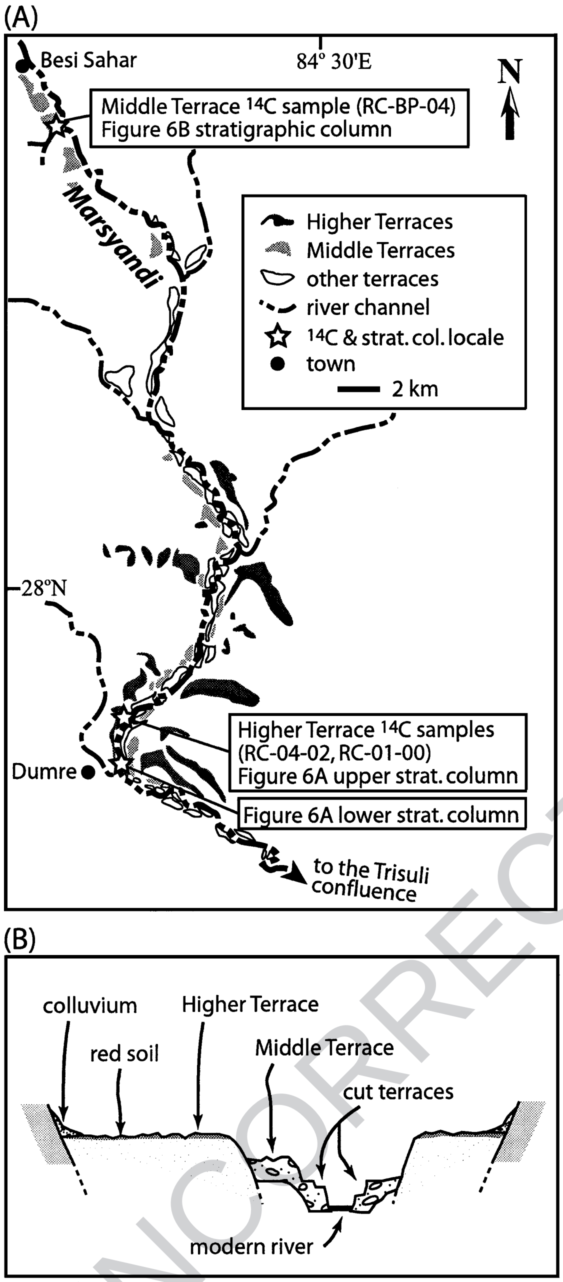

Fig. 4. (A) Intramontane valley depositional terraces. (B) Schematic cross-section of the intramontane valley (after Yamanaka and Iwata, 1982).

meters thick (Lavé and Avouac, 2001). The southern intramontane alluvial reach is flanked by fill terraces that are up to several square kilometers in extent with surfaces up to 170 m above the modern river (Yamanaka and Iwata, 1982).

3. Methodology

The Marsyandi River incised 1.5–2 mm/year over the last 5–10 My. Over shorter time periods, incision may have been faster, slower, or even stopped during times of alluviation. A key problem is how to define, date, and interpret the range of rates and processes which the river has experienced. Here we use fluvial terraces, straths, and radiometric dating to unravel Marsyandi's history of incision and aggradation.

3.1. Fill terraces study

Terrace elevation profiles were determined by altimeter, and laser finder field studies, along with analyses of topographic maps, airphotos, and digital elevation models (DEM). To determine terrace genesis, we measured decimeter-scale stratigraphic profiles and collected organic fragments for radiocarbon dating.

Terrace-surface topographic profiles that are steeper or gentler than the modern river gradient can reveal spatially varying incision rates or temporally changing sediment flux. Locations and geometries of the major terraces were ascertained from airphoto analysis and field observations. Longitudinal profiles of major terraces south of the Greater Himalaya were determined by spot height measurements on 1:25,000-scale topographical maps (Nepal and Finland, 1998). In a few cases where no spot heights were available, longitudinal terrace altitudes were interpolated between the 20-m contours. The longitudinal river profile was derived directly from map contours. In the Greater Himalaya, terrace heights were determined by altimeter or laser range finder and the river profile was taken from 1:50,000-scale topographical maps (Nepal and Finland, 2001). Locations were determined by hand-held GPS.

3.2. Cosmogenic radionuclide dating

On 10^4–10^5-year timescales, incision rates can be determined from cosmogenic radionuclide (CRN) dating of fluvially carved surfaces (see Gosse and Phillips, 2001 for a detailed discussion of CRN theory and application). If fluvially etched surfaces are not removed by incremental erosion or buried by landslides, CRN exposure ages of these surfaces, when combined with their height above the modern river, can yield average bedrock incision rates for the river. We used ^{10}Be and ^{26}Al concentrations to determine exposure ages of fluvially carved surfaces in order to measure spatial and temporal variations in river incision.

Thirty-one fluvially sculpted, bedrock knobs and small (< 50 m) straths were sampled along the Marsyandi from 28 to 124 m above the modern river (Fig. 1). Cosmogenic radionuclide production decreases exponentially with depth such that, 1 m into the rock, production is < 18% of its surface value. Because of this, we collected most samples from small fluvial surfaces carved into hillslopes >30°, so that any locally derived debris (such as from landslides) should have been rapidly shed off the steep slopes. Areas affected by tributary runoff were also avoided because they could have experienced fluvial erosion subsequent to main channel occupation. Due to limited available sites, some samples were taken from substandard sites with an increased likelihood of cosmogenic shielding by regolith that could lead to an underestimation of the true time since formation. All the samples are from altitudes (< 2000 m) where snow cover is not considered a problem now or in the past (Pratt et al., 2002b).

Where possible, two samples were collected from each surface. In order to assess the temporal and spatial variability of incision rates, samples were collected over the greatest possible latitudinal extent, and vertical arrays of samples were collected at different heights above the modern river. We used an altimeter, handheld GPS, and laser range finder to determine height above modern river, altitudes, and locations.

Seventeen samples were prepared for ^{10}Be and ^{26}Al analysis at Dartmouth College, NH, according to methods outlined by Kohl and Nishiizumi (1992) and Ditchburn and Whitehead (1994). Isotope concentrations were measured at Lawrence Livermore National Laboratory (LLNL), Center for Accelerator Mass Spectrometry. We calculated final exposure ages with a Matlab program provided by LLNL (Farber et al., 2001), which uses production rates of 5.1 and 31.1 atoms/g/year for ^{10}Be and ^{26}Al, respectively (Stone, 2000), and corrects for the non-dipole magnetic field (Dunai, 2000), latitude, altitude, sample depth, and topographic shielding. Average ages ($\pm 2\sigma$) were determined from an error-weighed mean using Isoplot (Ludwig, 1999).

4. Results and interpretation

4.1. Fill terraces

4.1.1. Stratigraphy, genesis, and timing

Two major terrace sequences, previously termed the Higher and Middle Terraces (Yamanaka and Iwata, 1982; Lavé and Avouac, 2001), are preserved along

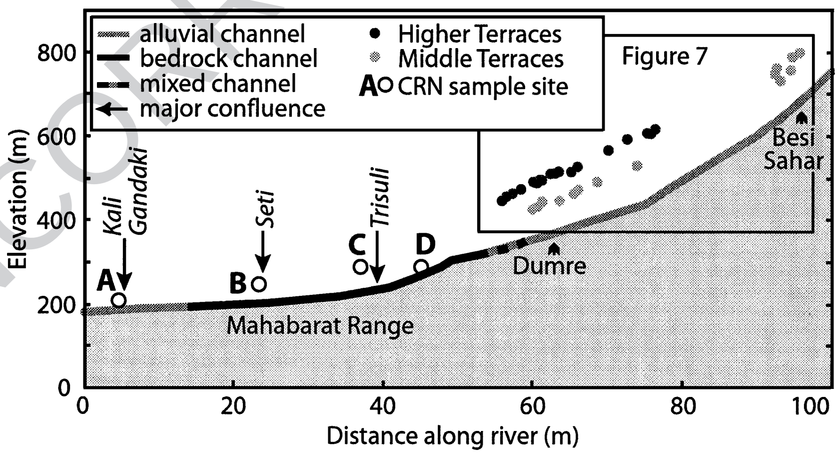

Fig. 5. Long-river profile of the Higher Terraces, Middle Terraces, and modern Marsyandi River derived from topographical maps. Fig. 7 graphs the terrace heights above the modern river.

the intramontane alluvial reach between the Greater Himalaya and the Mahabarat (Figs. 1 and 4). The Higher Terraces can be traced for 25 km and are 110–170 m above the modern river. The Middle Terraces are 70–120 m above the river and extend for 40 km (Fig. 5). Based on our measured sections, ~ 75% by volume of the Higher Terraces is composed of 1–20-m-thick, heterolithic, matrix-supported conglomerates with angular to subangular clasts up to 1.5 m in diameter; whereas ~ 25% is composed of 1–10-m-thick, heterolithic, partially clast-supported conglomerates with imbricated subrounded to rounded clasts up to 30 cm in diameter (Fig. 6A). The upper half of the Higher Terraces also contains a few 0.1–2-m-thick sand and silt beds, some with organic remains. Layers that display grading are normally graded. The top 5 m of the terrace fill has weathered to a dark red soil with a few highly weathered clasts.

We interpret the angular matrix-supported beds to be debris-flow deposits and the rounded clast-supported units to be of fluvial origin (Nichols, 1999). The fine-grained layers are interpreted to be paleosols and overbank deposits. Overall, the massive beds and coarse-grained material suggest rapid sedimentation

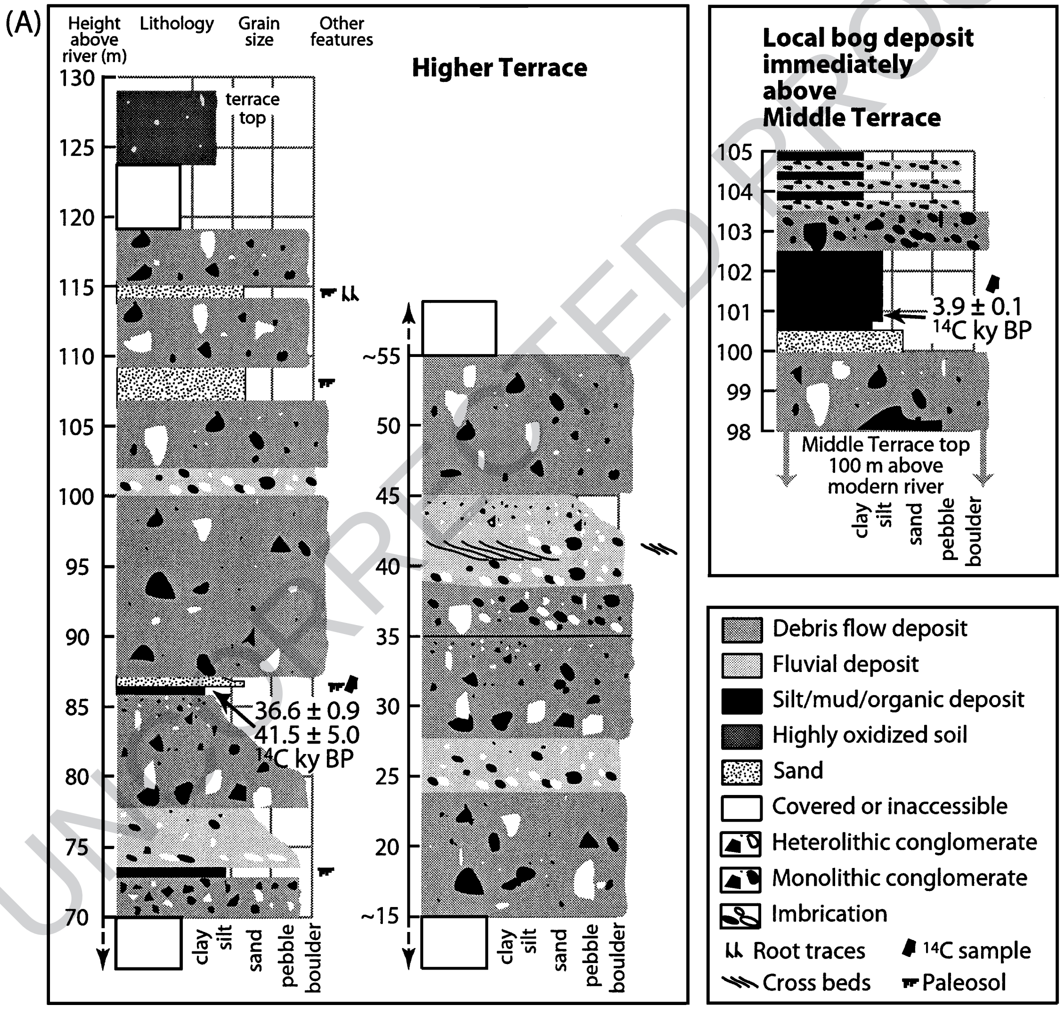

Fig. 6. Measured stratigraphic sections from (A) Higher Terrace ^{14}C sample site and a stratigraphically lower section ~ 2 km to the south on the same terrace; and (B) ^{14}C sample site from a bog immediately above the Middle Terrace (see Fig. 4 and Table 1 for location information).

events followed by some fluvial reworking. The heavily weathered capping soil indicates that the Higher Terraces are significantly older than any of the lower terraces, all of which lack such soils. Two charcoal fragments (RC-04-02, RC-01-00) in a sandy silt layer 45 m below the top of a Higher Terrace and 85 m above the modern river yielded AMS dates of 36,610 ± 900 ky BP and 41.5 ± 5.0 ^{14}C ky BP (± 2σ), respectively (Table 1). We assign greater confidence to sample RC-04-02 because it was larger, less altered, younger, and has a lower uncertainty. However, use of either date places terrace aggradation in the same temporal window. If we assume that aggradation was rapid with respect to the time since terrace abandonment, these dates imply that the Higher terraces had aggraded by ~ 30–35 ky BP.

Most of the clasts source to Great Himalayan rocks, 20–40 km to the north, and thus demonstrate clearly (but surprisingly) that debris flows can travel these distances. The modern Marsyandi channel shows no evidence of regular deposition of 1–20-m-thick debris flows, so a profound change in sedimentation and/or preservation has occurred.

The Middle Terraces are composed of a massive, heterolithic, matrix-supported deposit containing Greater Himalayan Sequence augen gneiss boulders up to 5 m in diameter and displaying a preserved upper surface 70–120 m above the modern river. It is interpreted to be a single massive landslide deposit originating in the Greater Himalaya, probably up the Ngadi Khola tributary. A rough estimate places its volume at ~ 1.5 km^3. We conjecture that the sudden emplacement of the Middle Terraces dammed the Kaleni Khola, a small tributary of the Marsyandi 2 km south of Besi Sahar. Wood fragments near the bottom of the resulting bog (Fig. 6B) that directly overly the debris flow yielded an age of 3.9 ± 0.1 ^{14}C ky BP (± 2σ) (Table 1). Because our sample directly postdates the Middle Terrace deposit, this agrees with the dates 4.2 ± 0.1 and 4.3 ± 0.1 ^{14}C ky BP (± 1σ) from within the terrace (Yamanaka, 1982).

Between the Higher Terrace surface and the modern river are numerous, typically unpaired terraces. Many of these appear to be cut terraces incised into the Middle Terraces. Others could be local debris deposits or poorly preserved aggradational surfaces.

4.1.2. Terrace topographic gradients

The modern river has a gradient of 5.5 m/km along the Higher Terraces and steepens to 12 m/km by the upper end of the Middle Terraces. The Higher and Middle Terraces have surface slopes that are steeper than the modern river by 2.5 ± 0.4 and 0.9 ± 0.3 m/km, respectively (Fig. 7). We interpret the present surface of the Middle Terraces to be essentially the same as the surface of the massive debris flow that created it. We argue that less than one-third of the excess gradient of the Middle Terraces could be due to tectonic tilting. The Higher Terraces (~ 35 ky) are ~ 10 times older than the Middle Terraces (4 ky). If the entire excess gradient of the Higher Terraces (2.5 m/km) was due to tectonic tilting, then the tilting must have occurred at a mean rate of 0.07 m/km/ky. Assuming constant tilting rate, the 4-ky Middle Terraces could only have been tilted 0.28 m/km. Given a residual gradient of ≥ 0.6 m/km, the Middle Terraces

Table 1
^{14}C sample and sample site information[a]

Sample #	Latitude	Longitude	$\delta^{13}C_{PDB}$ (‰)	Date (^{14}C BP) [lab technique]	Site description
RC-04-02	27°59.120′N	84°25.496′E	– 12.3	36.6 ± 0.9 [AMS]	Charcoal from a silt layer 45 m below the Higher Terraces top along the main road about 2.5 km north of Dumre.
RC-01-00	"	"	– 12.4	41.5 ± 5.0 [AMS]	Same as above.
RC-04-00	28°12.894′N	84°23.083 E	– 28.7	3.9 ± 0.1 [conventional]	Wood from the base of a bog deposit along the Kaleni Khola ~ 50 m west of the road, ~ 2 km south of Besi Sahar.

[a] Errors are 2σ.

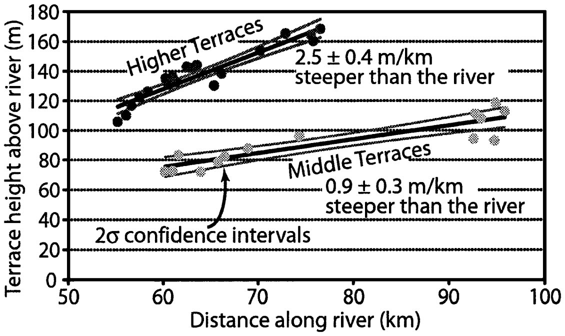

Fig. 7. Higher and Middle Terraces' height above river level. Regression lines shown with 2σ confidence intervals. The modern river gradient is 5.5 m/km along the High Terrace region and steepens to 12 m/km by the upper end of the Middle Terraces.

depositional surface gradient must have been steeper than the modern river gradient.

The Higher Terraces' steeper gradient could also be due to tectonic tilting and/or steeper depositional slopes. Deposits, such as the Higher Terraces, are preserved when sediment supply exceeds a river's carrying capacity. This excess sediment could have caused the channel to steepen to a new energy slope (Soni et al., 1980; Bennett and Bridge, 1995; Tucker, 1996; Alves and Cardoso, 1999).

Although sediment supply outstripped Marsyandi's transport capability during the Higher Terrace formation, present-day incision rates of ≥ 17 mm/year (≥ 70 m in 4 ky) into the Middle Terraces and the absence of sediment storage in the greater Himalaya demonstrate that the modern river is underloaded with sediment. The sediment-to-water-discharge ratio must have been considerably higher during aggradation of the Higher Terraces than it is now, so it is likely that some portion of the Higher Terraces' steeper gradient is due to an increased sediment flux, rather than tectonic tilting. Abrupt changes in the sediment-to-water discharge are aptly demonstrated in Holocene deposits of the Bengal

Table 2
Exposures ages and incision rates for polished fluvial surfaces on the Marsyandi River[a]

Sample ID	Height above river (m)	Altitude (m)	[^{10}Be] (10^3 atoms per g Qtz)	^{10}Be age (ka)	[^{26}Al] (10^3 atoms per g Qtz)	^{26}Al age (Ka)	Averaged exposure age (Ka)	Incision rate (mm/yr)
NP-102[b]	*23*	*210*	*10.8 ± 7.2*	*2.7 ± 1.8*	*6.4 ± 37.7*	*0.3 ± 3.1*	*2.1 ± 1.6*	*11 ± 8.5*
NP-104[b]	*45*	*245*	*2.2 ± 4.0*	*0.6 ±1.0*	*7.3 ± 6.4*	*0.3 ± 0.3*	*0.3 ± 0.3*	*140 ± 111*
NP-108	**48**	**270**	**133 ± 7**	37.5 ± 3.1	**887 ± 124**	**41.6 ± 6.4**	**38.7 ± 5.6**	**1.3 ± 0.1**[c]
NP-109	**49**	**270**	**130 ± 9**	**36.8 ± 3.3**	**962 ± 103**	**45.9 ± 5.6**		
NP-106[b]	**25**	**285**	**54.4 ± 10.0**	**14.2 ± 2.7**	**nm**[d]	**nm**	**14.2 ± 2.7**	**1.7 ± 0.3**
NP-110[b]	*31*	*1120*	*13.7 ± 4.0*	*1.9 ± 0.6*	*71.6 ± 34.2*	*1.7 ± 0.8*	*1.8 ± 0.5*	*16.2 ± 4.2*
NP-111	**81**	**1225**	**54.8 ± 5.8**	**6.8 ± 0.8**	**291 ± 42**	**5.9 ± 0.9**	**6.3 ± 0.6**	**12.8 ± 1.2**
NP-112	**43**	**1225**	**41.6 ± 6.4**	**5.9 ± 1.0**	**150 ± 139**	**3.5 ± 3.0**	**6.5 ± 1.6**	**6.6 ± 1.6**
NP-112B	**43**		**nm**	**nm**	**205 ± 142**	**4.8 ± 3.4**		
NP-113	**43**	**1225**	**50.5 ± 4.8**	**7.2 ± 0.8**	**285 ± 62**	**6.7 ± 1.5**		
NP-115	**76**	**1260**	**48.2 ± 5.6**	**6.5 ± 1.1**	**273 ± 111**	**6.1 ± 2.5**	**6.5 ± 1.0**	**11.7 ± 1.8**
NP-116	**124**	**1305**	**62.7 ± 5.4**	**7.3 ± 0.8**	**308 ± 64**	**5.9 ± 1.3**	**6.7 ± 0.5**	**18.4 ± 1.2**
NP-117	**123**	**1305**	**56.1 ± 4.0**	**6.6 ± 0.6**	**nm**	**nm**		
NP-121	**66**	**1535**	**71.4 ± 13.8**	**7.8 ± 1.6**	**nm**	**nm**	**7.8 ± 1.6**	**8.5 ± 1.7**
NP-123[b]	*89*	*1560*	*34.9 ± 9.4*	*3.5 ± 1.0*	*66.0 ± 89.4*	*1.1 ± 1.4*	*2.8 ± 0.8*	*32.3 ± 9.4*
NP-124	**110**	**1580**	**65.7 ± 5.2**	**7.6 ± 0.8**	**nm**	**nm**	**7.6 ± 0.8**	**14.5 ± 1.5**
NP-127[b]	*68*	*1760*	*5.6 ± 4.2*	*0.9 ± 0.7*	*nm*	*nm*	*0.9 ± 0.7*	*75.1 ± 57.4*
NP-128	**28**	**1890**	**39.4 ± 6.4**	**3.8 ± 0.7**	**244 ± 46**	**3.8 ± 0.8**	**3.8 ± 0.5**	**7.2 ± 1.0**

[a] Final results were averaged for all samples at the same location. Bold type indicates samples being used in the analysis. Italicized ages were excluded, as explained in the text. NP-112 was measured twice for ^{26}Al and the two measurements were averaged. The average strath ages are error-weighted using Isoplot (Ludwig, 1999). Errors are 2σ. Cosmogenic nuclide production rates were 5.1 and 31.1 atoms/year/g Qtz, respectively.

[b] Denotes sample locations deemed poor while in the field.

[c] Gray box indicates useable incision rates (discussed in text).

[d]nm denotes no measurement made.

Delta, where Early Holocene deposition rates at least double the Late Holocene rates (Goodbred and Kuehl, 2000 #412). Such doubling of sediment flux is likely to cause both aggradation and river bed steepening (Bennett and Bridge, 1995).

4.2. Cosmogenic radionuclide dating—exposure ages and incision rates

Fourteen exposure ages of scoured fluvial surfaces were derived along the Marsyandi from a total of 17 samples (Table 2, Fig. 8, Appendices). Exposure ages were measured for all 17 samples with ^{10}Be and for 12 samples with ^{26}Al. Paired samples taken from the same surface were averaged to determine the surface's age.

Five of the samples returned untenably low exposure ages (Table 2, italics). All five had been designated in the field as substandard sample sites either because they were likely to have been buried by subsequent aggradational terraces or because of their positions on low-angle hillslopes that could have held local debris cover. We have excluded these five samples from the analysis. Of the 12 remaining samples, 11 were deemed good quality sample locations while in the field.

The useable exposure ages fall naturally into two main groups, those in the Mahabarat and those in the Greater Himalaya. In the Mahabarat, sites C and D yielded ages of 38.7 ± 5.6 (± 2σ) and 14.2 ± 2.7 ky, respectively (Fig. 8A). Exposure ages in the Greater Himalaya were much younger with a population ranging from 6.3 ± 0.6 to 6.7 ± 0.5 ky at sites F and G, two surfaces of 7.6 ± 0.8 and 7.8 ± 1.6 ky at site H, and a single surface record-

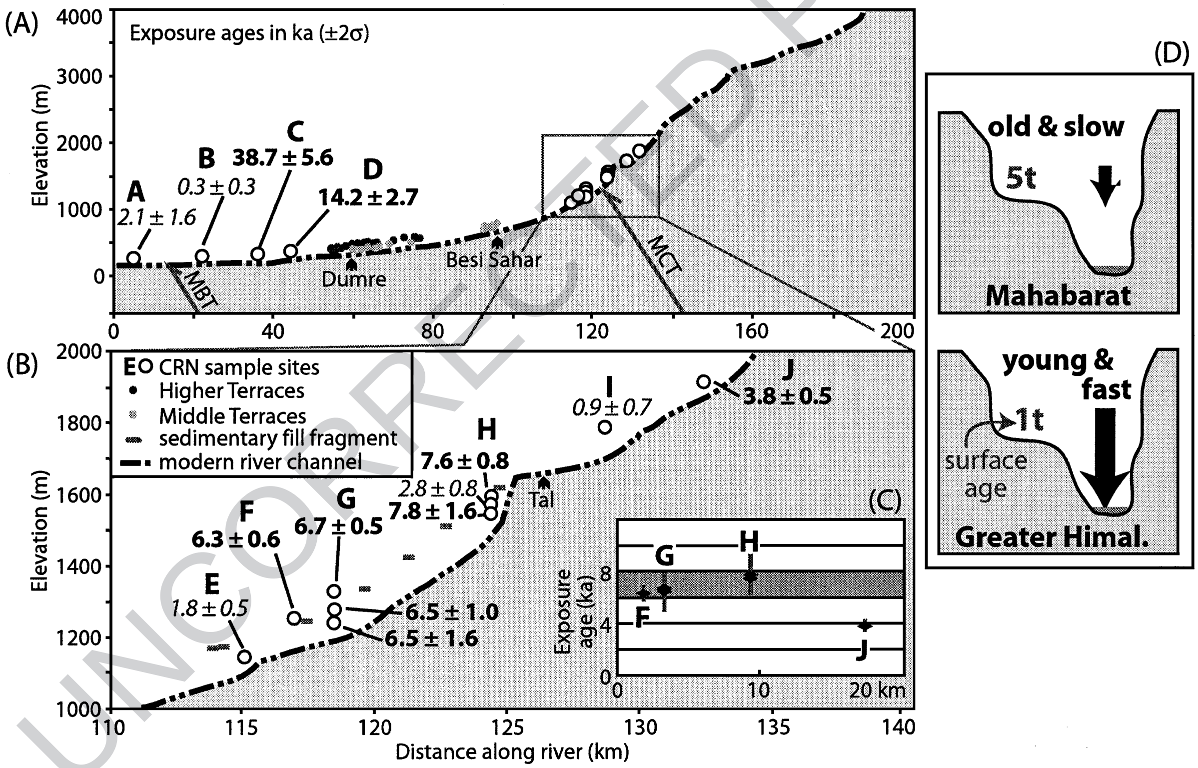

Fig. 8. (A) Site locations and exposure times of polished fluvial surfaces along the entire study region. (B) Close up of the Greater Himalayan sites. (C) Graph of tight grouping 8–6 ky exposure ages at sites F, G, and H. Bold type indicates samples being used in the analysis. Italicized ages were excluded, as explained in the text. MCT, Main Central thrust; MBT, Main Boundary thrust. (D) Exposure age versus incision rate relationship: older exposure ages (5t) at the same height above the river imply slower incision rates in the Mahabarat Range; younger exposure ages (1t) imply faster incision rates in the Greater Himalaya; "t" = bedrock surface exposure age.

ing an age of 3.8 ± 0.5 ky at site J (Fig. 8B) (Pratt et al., 2002a).

Assuming that incision and rock uplift are roughly balanced, a surface in a region of slow uplift should be older than a surface at the same height above the bed in a rapidly uplifting zone (Fig. 8D). The surfaces in the Mahabarat, with ages of 38.7 ky at 49 m and 14.2 ky at 25 m, are considerably older than surfaces of similar heights in the Greater Himalaya, with ages of 6.5 ky at 43 m and 3.8 ky at 28 m. With its lower topography, hillslope angels (Fig. 3), and seismicity (Pandey et al., 1995, 1999), the Mahabarat Range might be expected to have slower rock uplift rates. From exposure ages at sites C and D, the Marsyandi River has a calculated incision rate of ~ 1.5 mm/year (Fig. 9A) in the Mahabarat Range.

If a river is steadily cutting into bedrock, one would expect exposure ages of pristine fluvial features to be older on surfaces higher above the river (Fig. 10). Given the vertical spacing of sample sites at locations G and H (Table 2; Fig. 8B), we would expect an approximately threefold difference in exposure ages from the highest and lowest sites, if steady incision is assumed. This is not what we observed; instead, all eight samples at sites F, G, and H returned nearly identical exposure ages of 6.3–7.8 ky (Fig. 8C).

If these superposed ages are interpreted simply as a function of bedrock incision, they would require abrupt changes in incision rates: 80 m of incision would have occurred between 8 and 6 ky BP (~ 40 mm/year); whereas only 40 m of incision would have occurred in the subsequent 6 ky (~ 7 mm/year). No reasonable mechanism appears likely to have caused the 40 mm/year incision or a sixfold change in incision rate throughout this region. Instead, we interpret these ages to imply that the river had incised to at least the level of the lower sampled surfaces (40 m above the modern river) sometime before 8 ky BP (Fig. 10) (Pratt et al.,

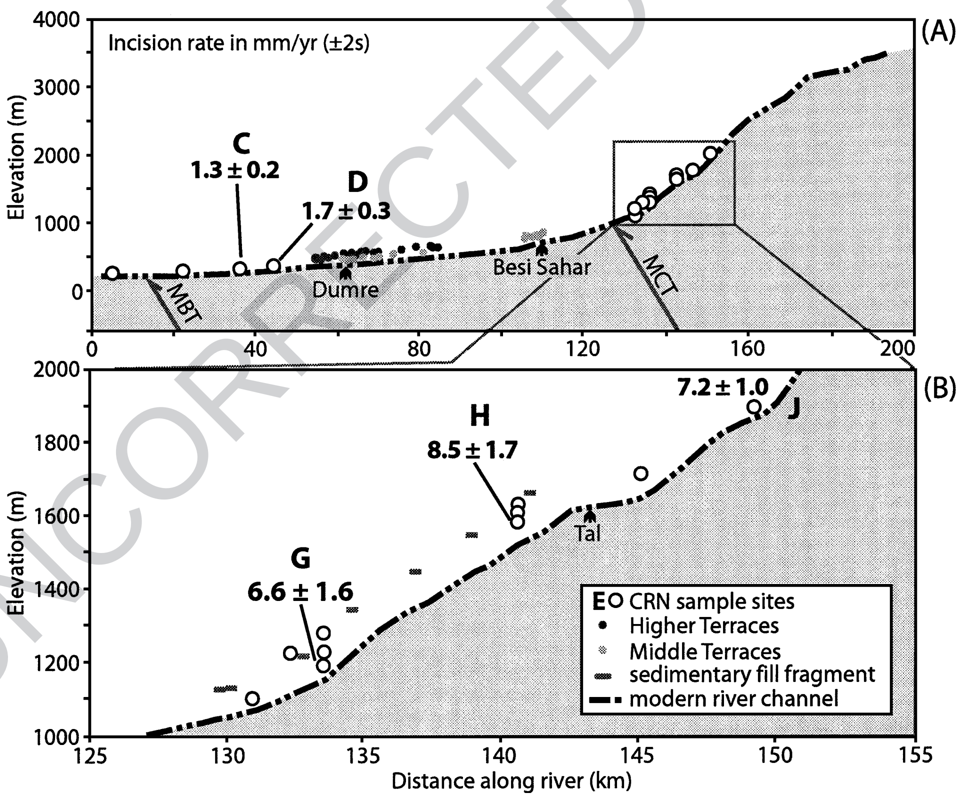

Fig. 9. (A) Maximum incision rates along the entire study region. (B) Close up of the Greater Himalayan sites.

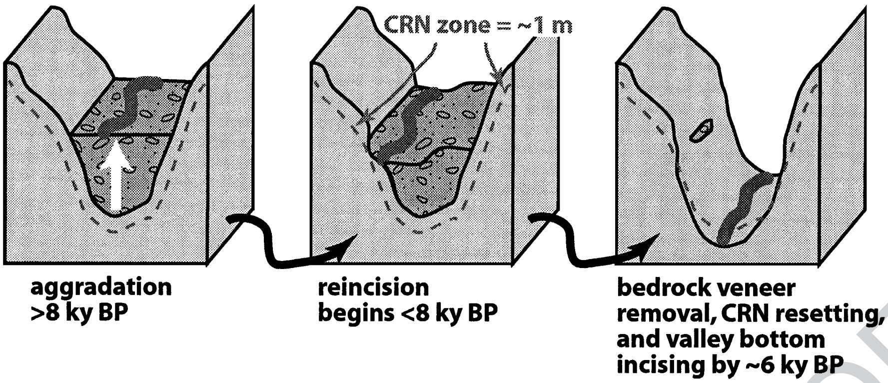

Fig. 10. Schematic drawing of cosmogenic radionuclide (CRN) resetting in Marsyandi's Greater Himalayan reach. River valley aggrades with alluvial fill >8 ky BP. Between 8 and 6 ky BP, the alluvium and a bedrock veneer ≥ 1 m thick are removed from the valley, resetting the surface rock's CRN concentration to zero. Fragments of fluvial deposits support the idea that alluvium reached >100 m above the modern river level.

2002a). By ~ 8 ky BP, the Marsyandi had alluviated its channel to ~ 120 m above the modern river level. Subsequently, as the river re-incised the valley fill, the alluvium and at least 1 m of the bedrock wall were removed from the valley between 8 and 6 ky BP. Cosmogenic nuclide production rates attenuate with depth in a rock, such that erosion of the upper 1–2 m of rock during rapid removal of the valley alluvium would "reset" the rock cosmogenically. Along the bedrock reach of the Marsyandi, isolated deposits of bedded sands and rounded cobbles 100–120 m above the modern river support the idea that alluvium once reached this level (Fig. 8B).

The cosmogenic resetting event renders most, but not all, of the sampled Greater Himalayan surfaces useless for calculating bedrock incision rates. At site J, the exposure age of 3.8 ky postdates the inferred alluviation and resetting. The age and height (28 m above the modern river) yield a vertical incision rate of ~ 7 mm/year (Fig. 9B). The lowest sites in the vertical sampling arrays (G1 and H1) predict similar incision rates since ~ 6.5 ky of 8.5 and 6.6 mm/year, respectively, and could have been at or near river level when alluviation began. Because the height of H1 (66 m above the river) is 50% greater than that of G1 (43 m), H1 is more likely to have been above the valley bottom when alluviation began, and its apparent higher rate is not problematic. From these data, we conclude that bedrock incision rates by the Marsyandi River have been as high as 7 mm/year in the Greater Himalaya during the Holocene and ~ 1.5 mm/year in the Mahabarat since later Pleistocene times.

5. Discussion

5.1. Significance of the cosmogenic radionuclide dates

Although CRN dating provides an unparalleled means to determine exposure ages, several uncertainties are poorly quantified. We have not included the uncertainties associated with nuclide production rates, which are currently 6–10% (Nishiizumi et al., 1989; Dunai, 2000; Gosse and Phillips, 2001). Our AMS analytical errors were often >10% ($\pm 2\sigma$); and multiple samples from individual surfaces yield a range of ages. The greatest variation is found at site G1; these ages extend from 3.5 ± 3.0 to 7.2 ± 0.8 ky with an error-weighted mean at 6.5 ± 1.6 ky (Table 2). Even though ^{10}Be and ^{26}Al dating does not yield exact ages for each surface, it demonstrates that all surfaces at sites F and G have statistically indistinguishable ages and probably formed within <2 ky of each other.

Further upstream, at site H, the surface ages center at 7.7 ky BP, but with error ranges that overlap those of F and G (Fig. 8C). This more northern site may have retained some cosmogenic nuclides from a previous exposure, or it may have been formed earlier. The sample surfaces at F and G were flatter and more extensive, whereas site H contained only fluvially rounded knobs. Regardless, all of these surfaces were probably carved within < 2 ky of each other.

Incision of ~100 m of fill in 1–2 ky requires that every 100 years, the river removes 5–10 m of fill. Can ~1 m of bedrock be eroded in the 100 years it took the river to lower past a given spot? The required horizontal bedrock incision rates are high (~10 mm/year), but comparable rates have been documented elsewhere (e.g. 2–10 mm/year: Burbank et al., 1996; 10–100 mm/year: Whipple et al., 2000; 4–17 mm/year: Hartshorn et al., 2001). Moreover, we preferentially sampled in areas with well polished, fluted, or scoured surfaces, which likely experienced the maximum erosion and resetting during incision (Pratt et al., 2002a).

5.2. Implication for determining bedrock river incision rates

The observed cosmogenic resetting along the Greater Himalayan reach highlights the difficulty in obtaining bedrock river incision rates from exposure ages in such dynamic environments. Surfaces should be sampled as high above the river as possible, not only to extend the study farther back in time but also to attempt to rise above the perturbations caused by alluviation and resetting cycles. Little confidence can be assigned to an incision rate unless a vertical sequence of at least two surfaces returns the same rate. We obtained two, vertically separated surfaces with similar incision rates in both the Mahabarat (1.3 and 1.7 mm/year) and Greater Himalaya (6.6 and 7.2 mm/year), lending credence to their significance over those exposure times.

5.3. Mechanisms of alluviation

At timescales >10^5 years, the Marsyandi incises into the Himalayan bedrock. However, this study demonstrated that at least three alluviation events have filled portions of the Marsyandi to ≥100 m during Quaternary times: the ~35-ky Higher Terraces; the ~8-ky Greater Himalayan alluviation; and the 4-ky mass flow deposits of the Middle Terrace. An understanding of the erosion process on shorter timescales requires an explanation of the mechanism(s) behind these aggradational episodes.

The Middle Terrace formed in a single massive landslide, probably triggered by a seismic event, and is thus not indicative of any longer-term forcing such as climate change. Although such flows have been noted elsewhere (e.g. Fort, 1988), the mechanics of how >1 km^3 of rock can travel ≥40 km is certainly worthy of further study. Presumably, some condition (such as high potential energy due to initiation ≥5 km ASL, high water content, or large volume) raises the internal pore pressure high enough that it overcomes resistance due to grain friction at the margins (Major and Iverson, 1999).

The other alluviations could result from climate-stimulated changes in sediment flux, baselevel changes, or landslide dams. Both the steeper surface slope and ≥110–170 m accumulation of the Higher Terraces can be explained by a climate-induced increase in relative sediment flux. A 110-m baselevel rise in the Mahabarat could lead to upstream aggradation, but this scenario requires activity on the Main Boundary thrust to have accelerated, outpacing the Marsyandi's incision capability for 10^4–10^5 years, and then slowed to ≤1.7 mm/year during the past 40 ky. These changing rates seem especially unlikely given that the entire Holocene India–South Tibetan convergence rate (Bilham et al., 1997) has been accommodated by motion on the Main Frontal thrust (not the Main Boundary thrust), and shortening rates have been nearly constant over the past 10 ky (Lavé and Avouac, 2000). An increase in sediment discharge (relative to water discharge) is far more likely to cause river aggradation, and a regional climate change could accomplish it by changing the erosion rate and/or the precipitation.

A change in climate is also the least complicated explanation for the Early Holocene alluviation and resetting event in the Greater Himalaya (Pratt et al., 2002a) and the associated fluvial terrace fragments (Fig. 8). Multiple, temporally close slides could account for the 15-km extent and >600-m vertical spread of the observed CRN site and fill deposits, but this is improbable without climatic or tectonic forcing. No field evidence exists for a massive landslide dam of this proportion. Climate change offers a more viable, regionally extensive mechanism for alluviation.

Does climate appears to have shifted substantially at these times? Summer monsoons dominate the climate in the central Himalaya, and there is mounting evidence from marine cores that the monsoons strengthened 9.5–5.5 and 50–35 ky BP (Clemens et al., 1991; Overpeck et al., 1996; Schulz et al., 1998) (Fig. 11). Paleoclimate records from paleolake cores in both Tibet (Gasse et al., 1996) and India (Enzel et al., 1999) also support the idea that 9.5–5.5 ky BP was a wetter time.

Intensified monsoons could increase the denudation rate by raising the pore pressure in the subsurface, which destabilizes hillslopes and increases landsliding, thereby releasing a pulse of sediment (Pratt et al., 2002a). Glaciers are potent erosive agents (Hallet et al., 1996), and Himalayan glaciers may expand to their maximum extents during intensified monsoons (Gillespie and Molnar, 1995; Benn and Owen, 1998; Phillips et al., 2000), thereby contributing additional sediment. Climatic change, probably in the form of monsoon intensification, is the mostly likely mechanism behind the ~35-ky Higher Terraces and the ≥8-ky Greater Himalayan alluviations. Goodbred and Kuehl (2000) observed a doubling of the deposition rate in the central and eastern Himalayan sediment sink, the Bengal Fan, from 11 to 7 ky BP—an observation consistent with our model. Intensified monsoons increase river discharge. Sediment supply must have grown by an even greater amount or the river would have eroded more rapidly rather than alluviate.

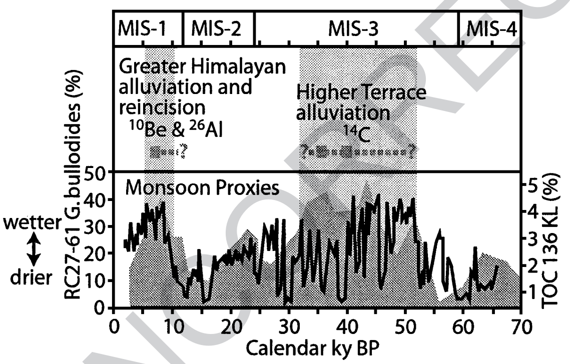

Fig. 11. Correlation of monsoon proxies from Arabian Sea sediment cores with this study. Dashed gray lines indicate times of Marsyandi alluviation as determined from ^{10}BE, ^{26}A1, and ^{14}C dates (gray squares). Relative SW Asian monsoon intensity shown by abundance of upwelling indicator G. bulloides (solid gray polygon; Clemens et al., 1991) and total organic carbon (black line; Schulz et al., 1998). Times of maximum monsoon precipitation are shaded. Marine isotope stages (MIS) 1–4 shown on top. Modified from Phillips et al. (2000).

The preserved reach of Higher Terraces has an estimated volume of ~3.5 km^3 (assuming a triangular cross-section). Depending on how far the terraces originally extended, the total volume could have been >8 km^3. If the Marsyandi catchment (4800 km^2) is eroding at ~2 mm/year, it should be producing 0.01 km^3/year of sediment. Thus, the material trapped in the Higher Terraces only represents 350–800 years of gross sediment flux. If the terraces accumulated over 10–15 ky, the stored material represents <2–8% of the material eroded during this time. The percentage drops further if one assumes the erosion rate increased above the million-year average of 1.5–2 mm/year during this time of higher sediment flux. Therefore, even in times of accumulation, majority of the sediment is not stored, but passed downstream.

5.4. Preservation of sedimentary deposits

A climate-induced increase in sediment supply should lead to region-wide deposition in the river valley; yet we observed only limited lateral evidence of past alluviation. The remaining Higher Terraces extend for just 25 km, but must have once filled the valley into both the Mahabarat and Greater Himalayan ranges. We conclude that the preservation of the Higher Terraces is indicative of lower tectonic and erosive activity in the intramontane reach.

As the most easily eroded features, sedimentary deposits are quickly removed in regions of rapid rock uplift and active erosion. Steep hillslopes and narrow valleys are primary indicators of rapidly incising regions where the hillslopes adjust to downcutting through landsliding. Slopes in the Greater Himalaya and Mahabarat are at or close to threshold for failure with mean slopes of 32° and 27°, respectively (Fig. 3C). The Higher Terraces' modern extent precisely corresponds to a region of wider valleys, a gentler river gradient (Fig. 5), and average hillslopes at just 19° (Fig. 3C), even if all terrace surfaces (slopes

< 10°) are removed from the calculation. If the fraction of slopes < 10° provides a rough proxy of relative erosion rates, the intramontane region stands out as a zone of slower erosion (Fig. 3D). Lithologic changes do not correspond to these changes in average hillslope angle or river gradient.

The preservation of the Higher Terraces and the adjacent hillslope geometry suggests a lower rate of river incision and rock uplift across the intramontane valley. The hillslope angles also suggest that this reach is experiencing low rates of rock uplift. Any differential tectonic activity along the length of the Higher Terraces is insignificant compared to differences between this intramontane valley and the surrounding region.

At present, only in the Greater Himalaya have we recognized sediments associated with the ~8 ky alluviation event. Presumably, deposition also occurred in the intramontane valley, but we have not yet located such deposits. Most likely, they were either overrun by the Middle Terrace 4 ky massive landslide deposit or were rapidly incised and removed during the 6-ky incision event seen in the Greater Himalaya.

5.5. Climate change implications for channel elevation

Using rates and timescales of river erosion and deposition, we can estimate the dynamic fluctuations of Marsyandi's channel heights. If a topographic steady state prevails over timescales of 10^5–10^6 years, rivers in actively deforming orogens can be considered fixed with respect to the geoid (Burbank et al., 1996). Elevation added through rock uplift is balanced by river incision. This model cannot be

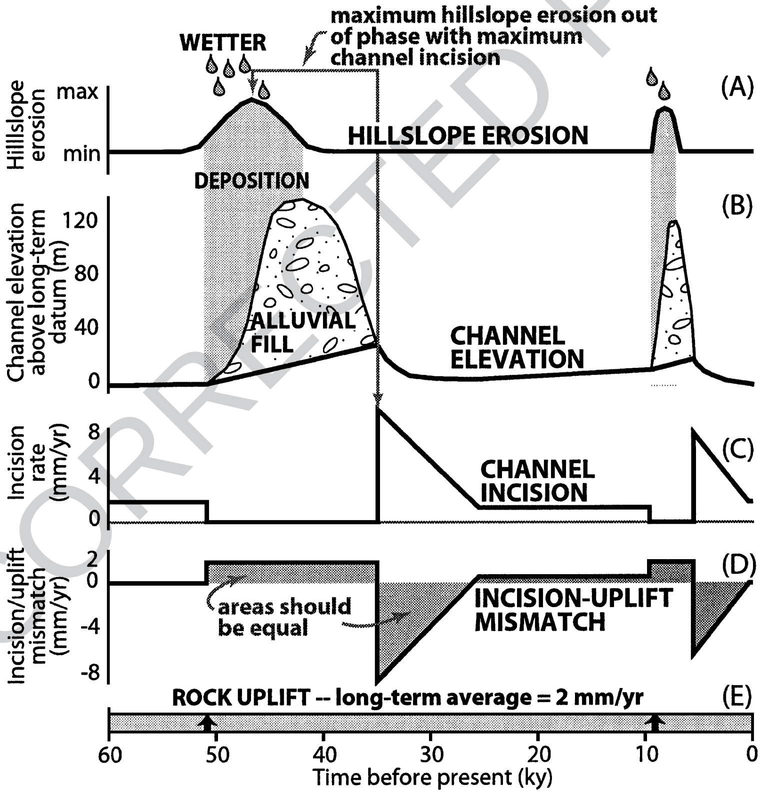

Fig. 12. Schematic drawing of river channel elevation through periods of alluviation and incision: (A) hillslope erosion; (B) channel elevation; (C) channel incision rate; (D) the mismatch between incision and rock uplift rates; and (E) long-term rock uplift rate. The uplift is assumed to be constant in order to illustrate the effects of erosion and deposition. In reality, this climate-driven modulation could be imprinted on top of rock uplift variations.

applied over the 10^4–10^5-year scales of alluviation and increased incision observed in this study. While Marsyandi's bedrock channel is shielded with sediments, incision is zero; but rock uplift will continue to elevate the channel (Fig. 12B). When the alluvium is flushed out and the bedrock is re-exposed, the bedrock channel gradient should be steeper; and the river should initiate a period of more rapid incision before slowing to a long-term average (Fig. 12C).

The exact shape of the incision rate curve is speculative, so it is shown here as a simple linear change through time. The curved could possibly be more sinusoidal with a maximum channel incision at a time of optimum tool availability (Sklar and Dietrich, 2001). This model (Fig. 12) implies that over a certain 1000-year interval, incision rates could spike even higher than 7 mm/year, but that over times of $\geq 10^4$ year, average incision rates would be ≤ 7 mm/year. If we assumed that Late Holocene incision was ~ 7 mm/year, that rock uplift has been 1.5–2 mm/year, and that Holocene alluviation only lasted 2–3 ky, then the river level must either have been above the predicted steady-state (10^5 year) level at the beginning of the Holocene (as shown in Fig. 12C) or it is lower than a long-term average now. A modest, < 1 mm/year, mismatch (Fig. 12D) between the channel incision rate and rock uplift rate will result in tens of meters of change in channel elevation over 10^4-year timescales.

If sediment flux increases, as we suspect it does during Asian monsoon intensification, erosion on the hillsides should be out of phase with the incision in the river channel (Fig. 12A). Heightened erosion on the hillslopes leads to filling of the valley floor and a cessation of river incision. When the hillslope erosion slows, the river can clear out the accumulated alluvium and begin a period of intensive incision. These punctuated cycles of aggradation and incision are only brought into focus if we observe the dynamic swings of the erosion process on shorter, nonequilibrium timescales.

6. Conclusions

Whereas actively deforming landscapes may be at equilibrium with erosion balancing rock uplift over million-year timescales, a closer look at the Marsyandi River system in the central Himalaya reveals the extent of disequilibrium over shorter periods. Climate change drives fluctuations in water and sediment discharge that cause the river channel to fluctuate between ~ 7 mm/year of bedrock incision and more than 100 m of deposition. Although these deposits can be surprising in their emplacement (debris flows traveling ≥ 40 km) and thickness (up to ≥ 170 m), at least the Higher Terraces represent only a small fraction (2–8%) of the total sediment which was denuded from the Marsyandi catchment during their deposition. At $>10^5$ year timescales, river incision rates define local baselevel lowering and hence the regional denudation rate. However, on the scale of thousands of years, the time of maximum river incision and hillslope denudation may be out of phase with each other. The elevation of the river channel must rise in response to continued rock uplift during times when the valley bottom is overwhelmed with alluvium and no bedrock incision can occur. All these factors point to a system with highly dynamic changes about some long-term, theoretical equilibrium. During efforts to quantify orogenic and geomophic rates, it is important to recognize the size, nature, and timing of landscape disequilibrium. Perceptions of Himalayan geomorphic processes might be quite different had we first observed the system during a time of major alluviation. This study highlights the need for continuing quantification of the role of climatic forcing on landscape development, rates, and processes.

Acknowledgements

We thank Daniel Farber for early access to his cosmogenic shielding program and Robert Finkel for accommodating our samples in a short time frame (Lawrence Livermore National Laboratories). Financial support came from the Continental Dynamics program at NSF (EAR-99-09647). We wish to thank the Department of Hydrology and Meteorology for excellent logistical support. Our gratitude to R. Alley, R. Slingerland, and B. Farrow for stimulating discussions on landsliding, monsoons, and fluvial sedimentation. The manuscript was greatly improved by thoughtful comments from W. Dietrich and an anonymous reviewer.

Appendix A

Table 1A
^{10}Be and ^{26}Al additional sample information[a]

Site	Sample #	Latitude (°N)	Longitude (°E)	River width at high water (m)	River slope	Description
A	*NP-102*[b]	*27°44.060′*	*84°25.586′*	*225*	*0.001*[c]	*pebbly sandstone strath*
B	*NP-104*[b]	*27°49.208′*	*84°27.199′*	*100*	*0.002*[c]	*quartz vein in rounded knob of schist*
D	**NP-106**[b]	**27°53.400′**	**84°32.439′**	**33**	**0.005**[c]	**rounded knob of quartzite**
C	**NP-108**	**27°50.693′**	**84°33.436′**	**63**	**0.003**[c]	**quartzite strath**
C	**NP-109**	**27°50.693′**	**84°33.436′**	**63**	**0.003**[c]	**quartzite strath**
E2	*NP-110*[b]	*28°23.243′*	*84°24.120′*	*43*	*0.026*	*quartz vein in flat mica–schist surface*
F	**NP-111**	**28°24.038′**	**84°24.550′**	**30**	**0.035**	**small strath of mica–schist**
G1	**NP-112**	**28°24.785′**	**84°24.455′**	**30**	**0.016**	**rounded knob of fine-grain gneiss**
G1	**NP-113**	**28°24.785′**	**84°24.455′**	**30**	**0.016**	**rounded knob of fine-grain gneiss**
G2	**NP-115**	**28°24.785′**	**84°24.455′**	**30**	**0.016**	**rounded knob of fine-grain gneiss**
G3	**NP-116**	**28°24.879′**	**84°24.423′**	**30**	**0.016**	**quartz vein in small strath of gneiss**
G3	**NP-117**	**28°24.879′**	**84°24.423′**	**30**	**0.016**	**quartz vein in small strath of gneiss**
H1	**NP-121**	**28°27.118′**	**84°22.582′**	**31**	**0.098**	**sm. round knob of medium-grain gneiss**
H2	*NP-123*[b]	*28°27.118′*	*84°22.582′*	*31*	*0.098*	*sm. flat surface of medium-grain gneiss*
H3	**NP-124**	**28°27.118′**	**84°22.582′**	**31**	**0.098**	**sm. round knob of medium-grain gneiss**
I	*NP-127*[b]	*28°29.274′*	*84°22.061′*	*22*	*0.042*	half-pothole of medium-grain gneiss
J	**NP-128**	**28°31.170′**	**84°21.521′**	**24**	**0.036**	**half-pothole of fine-grain gneiss**

[a] Bold type indicates sample being used in the analysis. Italicized ages were excluded, as explained in the text.
[b] Denotes sample locations deemed poor while in the field.
[c] Slope measured from 1:25,000 topographic map (all other measured in the field with laser range finder).

Appendix B

Table 1B
^{10}Be and ^{26}Al additional sample information[a]

Site	Sample #	Mass (g)	Be mass (mg)	Al Mass (mg)	Bulk density (g/cm^3)	Sample depth (cm)	Altitude/ latitude correction	Depth/ topography correction
A	*NP-102*[b]	*69.74*	*0.63*	*29.77*	*2.7*	*3*	*0.8*	*0.97*
B	*NP-104*[b]	*111.57*	*0.55*	*3.10*	*2.65*	*3*	*0.83*	*0.93*
D	**NP-106**[b]	**114.08**	**0.54**	**48.78**	**2.65**	**4**	**0.86**	**0.9**
C	**NP-108**	**104.43**	**0.50**	**40.17**	**2.65**	**2**	**0.86**	**0.88**
C	**NP-109**	**113.06**	**0.55**	**25.56**	**2.65**	**3**	**0.86**	**0.87**
E2	*NP-110*[b]	*113.88*	*0.52*	*15.51*	*2.7*	*2*	*1.65*	*0.84*
F	**NP-111**	**93.26**	**0.56**	**4.40**	**2.65**	**3**	**1.81**	**0.89**
G1	**NP-112**	**110.22**	**0.52**	**75.81**	**2.8**	**4**	**1.77**	**0.79**
G1	**NP-113**	**122.18**	**0.52**	**20.03**	**2.8**	**4**	**1.77**	**0.79**
G2	**NP-115**	**76.28**	**0.51**	**35.66**	**2.75**	**3**	**1.82**	**0.80**
G3	**NP-116**	**100.42**	**0.56**	**2.67**	**2.65**	**2**	**1.88**	**0.90**
G3	**NP-117**	**141.25**	**0.48**	**6.71**	**2.65**	**2**	**1.88**	**0.90**
H1	**NP-121**	**120.42**	**1.05**	**129.80**	**2.75**	**4**	**2.37**	**0.77**
H2	*NP-123*[b]	*64.98*	*0.48*	*17.92*	*2.75*	*3*	*2.41*	*0.82*
H3	**NP-124**	**102.63**	**0.53**	**162.87**	**2.75**	**3**	**2.44**	**0.7**
I	*NP-127*[b]	*93.33*	*0.49*	*36.24*	*2.75*	*2*	2.59	*0.46*
J	**NP-128**	**80.10**	**0.56**	**5.35**	**2.8**	**2**	**2.95**	**0.69**

[a] Bold type indicates sample being used in the analysis. Italicized ages were excluded, as explained in the text.
[b] Denotes sample locations deemed poor while in the field and excluded from the analysis.

References

Alves, E., Cardoso, A.H., 1999. Experimental study on aggradation. International Journal of Sediment Research 14 (1), 1–15.

Benn, D.I., Owen, L.A., 1998. The role of the Indian summer monsoon and the mid-latitude westerlies in Himalayan glaciation; review and speculative discussion. Journal of the Geological Society of London 155 (2), 353–363.

Bennett, S.J., Bridge, J.S., 1995. An experimental study flow, bedlord transport and bed topography under conditions of erosion and deposition and comparison with theoretical models. Sedimentology 42 (1), 117–146.

Bilham, R., Larson, K.M., Freymueller, J.T., Jouanne, F., Le Fort, P., Leturmy, P., Mugnier, J.L., Gamond, J.F., Glot, J.P., Martinod, J., Chaudury, N.L., Chitrakar, G.R., Gautam, U.P., Koirala, B.P., Pandey, M.R., Ranabhat, R., Sapkota, S.N., Shrestha, P.L., Thakuri, M.C., Timilsina, U.R., Tiwari, D.R., Vidal, G., Vigny, C., Galy, A., de Voogd, B., 1997. GPS measurements of present-day convergence across the Nepal Himalaya. Nature 386 (6620), 61–64.

Brewer, I.D., 2001. Detrital-mineral thermochronology: investigations of orogenic denudation in the Himalaya of central Nepal. PhD Dissertation, Pennsylvania State University, State College. 181 pp.

Bull, W.B., 1991. Geomorphic Responses to Climatic Change. Oxford University Press, New York. 326 pp.

Burbank, D.W., Leland, J., Fielding, E., Anderson, R.S., Brozovic, N., Reid, M.R., Duncan, C., 1996. Bedrock incision, rock uplift and threshold hillslopes in the northwestern Himalayas. Nature 379 (6565), 505–510.

Carson, M.A., Kirkby, M.J., 1972. Hillslope Form and Process. Cambridge Univ. Press, Cambridge, UK. 475 pp.

Clemens, S., Prell, W.L., Murray, D., Shimmield, G.B., Weedon, G.P., 1991. Forcing mechanisms of the Indian Ocean monsoon. Nature 353 (6346), 720–725.

Colchen, M., Le Fort, P., Pecher, A., 1986. Annapurna–Manaslu–Ganesh Himal. Centre National de la Recherche Scientifique, Paris, pp. 75–136.

Ditchburn, R.G., Whitehead, N.E., 1994. The separation of ^{10}Be from silicates. 3d Workshop of the South Pacific Environmental Radioactivity Association, pp. 4–7.

Dunai, T.J., 2000. Scaling factors for production rates of in situ produced cosmogenic nuclides: a critical reevaluation. Earth and planetary Science Letters 176 (1), 157–169.

Enzel, Y., Ely, L.L., Mishra, S., Ramesh, R., Amit, R., Lazar, B., Rajaguru, S.N., Baker, V.R., Sandler, A., 1999. High-resolution Holocene environmental changes in the Thar Desert, northwestern India. Science 284 (5411), 125–128.

Farber, D.L., Finkel, R., Meriaux, A., 2001. Unpublished Matlab program. Lawrence Livermore National Laboratory, Livermore, CA.

Fort, M., 1988. Catastrophic sedimentation and morphogenesis along the high Himalayan front; implications for palaeoenvironmental reconstructions. In: Whyte, P., Aigner, J.S., Jablonski, N.G., et al. (Eds.), The Paleoenvironment of East Asia from the mid-Tertiary. Centre of Asian Studies. University of Hong Kong, Hong Kong, pp. 170–194.

Gasse, F., Fontes, J.C., Van Campo, E., Wei, K., 1996. Holocene environmental changes in Bangong Co basin (western Tibet): Part 4. Discussion and conclusions. Palaeogeography, Palaeoclimatology, Palaeoecology 120, 79–92.

Gilbert, G.K., 1877. Report on the geology of the Henry mountains. U.S. Geographical and Geological Survey of the Rocky Mountain Region. U.S. Government Printing Office, Washington, DC. 160 pp.

Gillespie, A.R., Molnar, P., 1995. Asynchronous maximum advances of mountain and continental glaciers. Reviews of Geophysics 33 (3), 311–364.

Goodbred Jr., S.L., Kuehl, S.A., 2000. Enormous Ganges–Brahmaputra sediment discharge during strengthened early Holocene monsoon. Geology 28 (12), 1083–1086.

Gosse, J.C., Phillips, F.M., 2001. Terrestrial in situ cosmogenic nuclides: theory and application. Quarternary Science Reviews 20 (14), 1475–1560.

Hack, J.T., 1960. Interpretation of erosional topography in humid temperate regions. American Journal of Science 258-A, 80–97.

Hallet, B., Hunter, L., Bogen, J., 1996. Rates of erosion and sediment evacuation by glaciers; a review of field data and their implications. In: Solheim, A., Riis, F., Elverhoi, A., et al. (Eds.), Impact of Glaciations on Basin Evolution; Data and Models from the Norwegian Margin and Adjacent Areas. Elsevier, Amsterdam, pp. 213–235.

Hancock, G.S., Anderson, R.S., Whipple, K.X., 1998. Beyond power; bedrock river incision process and form. In: Tinkler, K.J., Wohl, E.E. (Eds.), Rivers Over Rock: Fluvial Processes in Bedrock Channels. American Geophysical Union, Washington, DC, pp. 35–60.

Hartshorn, K., Hovius, N., Slingerland, R., Dade, B., Lin, J., 2001. Linking observations and physics of fluvial bedrock erosion in an active mountain belt, east central Taiwan. Eos (Transactions American Geophysical Union) 82 (47), F585.

Hodges, K.V., 2000. Tectonics of the Himalaya and southern Tibet from two perspectives. Geological Society of America Bulletin 112 (3), 324–350.

Hodges, K.V., Parrish, R.R., Searle, M.P., 1996. Tectonic evolution of the central Annapurna Range, Nepalese Himalayas. Tectonics 15 (6), 1264–1291.

Kirby, E., Whipple, K.X., 2001. Quantifying differential rock-uplift rates via stream profile analysis. Geology 29 (5), 415–418.

Kohl, C.P., Nishiizumi, K., 1992. Chemical isolation of quartz for measurements of in-situ-produced cosmogenic nuclides. Geochimica et Cosmochimica Acta 56 (9), 3583–3587.

Lavé, J., Avouac, J.P., 2000. Active folding of fluvial terraces across the Siwaliks Hills, Himalayas of central Nepal. Journal of Geophysical Research, B, Solid Earth and Planets 105 (3), 5735–5770.

Lavé, J., Avouac, J.P., 2001. Fluvial incision and tectonic uplift across the Himalayas of central Nepal. Journal of Geophysical Research, B, Solid Earth and Planets 106 (11), 26561–26591.

Ludwig, K.R., 1999. Isoplot. Special Publication 1a. Berkeley Geochronology Center, Berkeley, CA.

Major, J.J., Iverson, R.M., 1999. Debris-flow deposition; effects of pore-fluid pressure and friction concentrated at flow margins. Geological Society of America Bulletin 111 (10), 1424–1434.

Molnar, P., 1987. Inversion of profiles of uplift rates for the geometry of dip-slip faults at depth, with examples from the Alps and the Himalaya. Annales Geophysicae. Series B: Terrestrial and Planetary Physics 5 (6), 663–670.

Nakata, T., 1989. Active faults of the Himalaya of India and Nepal. Special Paper—Geological Society of America 232, 243–264.

Nepal and Finland, 1998. Topographic map of Nepal. His Majesty's Government of Nepal and Government of Finland, Kathmandu, Nepal. 1:25,000.

Nepal and Finland, 2001. Topographic map of Nepal. His Majesty's Government of Nepal and Government of Finland, Kathmandu, Nepal.1:50,000.

Ni, J., Barazangi, M., 1984. Seismotectonics of the Himalayan collision zone; geometry of the underthrusting Indian Plate beneath the Himalaya. Journal of Geophysical Research, B, Solid Earth and Planets 89 (2), 1147–1163.

Nichols, G., 1999. Sedimentology and Stratigraphy. Blackwell Science, Malden, MA. 355 pp.

Nishiizumi, K., Winterer, E.L., Kohl, C.P., Klein, J., Middleton, R., Lal, D., Arnold, J.R., 1989. Cosmic ray production rates of ^{10}Be and ^{26}Al in quartz from glacially polished rocks. Journal of Geophysical Research, B, Solid Earth and Planets 94 (12), 17907–17915.

Overpeck, J., Anderson, D., Trumbore, S., Prell, W., 1996. The southwest Indian monsoon over the last 18 000 years. Climate Dynamics 12, 213–225.

Pandey, M.R., Tandukar, R.P., Avouac, J.P., Lavé, J., Massot, J.P., 1995. Interseismic strain accumulation on the Himalayan crustal ramp (Nepal). Geophysical Research Letters 22 (7), 751–754.

Pandey, M.R., Tandukar, R.P., Avouac, J.P., Vergne, J., Heritier, T., 1999. Seismotectonics of the Nepal Himalaya from a local seismic network. Journal of Asian Earth Sciences 17 (5–6), 703–712.

Pazzaglia, F.J., Knuepfer, P.L.K., 2001. The steady-state orogen; concepts, field observations, and models. American Journal of science 301 (4–5), 313–512.

Phillips, W.M., Sloan, V.F., Shroder Jr., J.F., Sharma, P., Clarke, M.L., Rendell, H.M., 2000. Asynchronous glaciation at Nanga Parbat, nothwestern Himalaya Mountains, Pakistan. Geology 28 (5), 431–434.

Porter, S.C., An, Z., Zheng, H., 1992. Cyclic Quarternary alluviation and terracing in a nonglaciated drainage basin on the north flank of the Qinling Shan, central China. Quarternary Research 38 (2), 157–169.

Pratt, B.A., Burbank, D.W., Heimsath, A.M., Ojha, T.P., 2002a. Impulsive alluviation during early Holocene strengthened monsoons, central Nepal Himalaya. Geology 30 (10), 911–914.

Pratt, B.A., Burbank, D.W., Putkonen, J., Ojha, T.P., 2002b. Climate implications of modern and paleo ELA's in the central Nepal Himalaya. Eos Transactions AGU, F319.

Schulz, H., von Rod, U., Erlenkeuser, H., 1998. Correlation between Arabian Sea and Greenland climate oscillations of the past 110,000 years. Nature 393 (6680), 54–57.

Schumm, S.A., 1973. Geomorphic thresholds and complex response of drainage systems. In: Morisawa, M. (Ed.), Fluvial Geomorphology. State Univ., Binghamton, NY, pp. 299–310.

Sklar, L., Dietrich, W.E., 2001. Sediment and rock strength controls on river incision into bedrock. Geology 29 (12), 1087–1090.

Small, E.E., Anderson, R.S., Repka, J.L., Finkel, R., 1997. Erosion rates of alpine bedrock summit surfaces deduced from in situ ^{10}Be and ^{26}Al. Earth and Planetary Science Letters 150 (3–4), 413–425.

Synder, N.P., Whipple, K.X., Tucker, G.E., Merritts, D.J., 2000. Landscape response to tectonic forcing; digital elevation model analysis of stream profiles in the Mendocino triple junction region, Northern California. Geological Society of America Bulletin 112 (8), 1250–1263.

Soni, J.P., Garde, R.J., Ranga Raju, K.G., 1980. Aggradation in streams due to overloading. Journal of the Hydraulics Division 106 (HY1), 117–132.

Stock, J.D., Montgomery, D.R., 1999. Geologic constraints on bedrock river incision using the stream power law. Journal of Geophysical Research, B, Solid Earth and Planets 104 (3), 4983–4993.

Stone, J.O., 2000. Air pressure and cosmogenic isotope production. Journal of Geophysical Research, B, Solid Earth and Planets 105 (10), 23753–23759.

Tucker, G.E., 1996. Modeling the Large-scale Interaction of Climate, Tectonics, and Topography. Technical Report Series, 96-003. Earth Systems Science Center. State College, PA. 267 pp.

Tucker, G.E., Slingerland, R., 1996. Predicting sediment flux from fold and thrust belts. Basin Research 8, 329–349.

Whipple, K.X., Synder, N.P., Dollenmayer, K., 2000. Rates and processes of bedrock incision by the upper Ukak River since the 1912 Novarupta ash flow in the Valley of Ten Thousand Smokes, Alaska. Geology 28 (9), 835–838.

Willett, S.D., 1999. Orogeny and orography; the effects of erosion on the structure of mountain belts. Journal of Geophysical Research, B, Solid Earth and Planets 104 (12), 28957–28982.

Yamanaka, H., 1982. Radiocarbon ages of upper Quaternary deposit in central Nepal and their geomorphological significance. Science Reports of the Tohoku University, Series 7 32 (1), 46–60.

Yamanaka, H., Iwata, S., 1982. River terraces along the Middle Kali Gandaki and Marsyandi Khola Central Nepal. Nepal Geological Society: Special Issue 2, 95–111.